National Renewable Energy Laboratory
A national laboratory of the U.S. Department of Energy
Office of Energy Efficiency & Renewable Energy
Innovation for Our Energy Future

Durability of Poly(Methyl Methacrylate) Lenses Used in Concentrating Photovoltaic Modules

Preprint

David C. Miller, Lynn M. Gedvilas, Bobby To, Cheryl E. Kennedy, and Sarah R. Kurtz

To be presented at SPIE 2010 Optics and Photonics Conference
San Diego, California
August 1-5, 2010

Conference Paper
NREL/CP-520-47604
August 2010

NREL is operated for DOE by the Alliance for Sustainable Energy, LLC Contract No. DE-AC36-08-GO28308

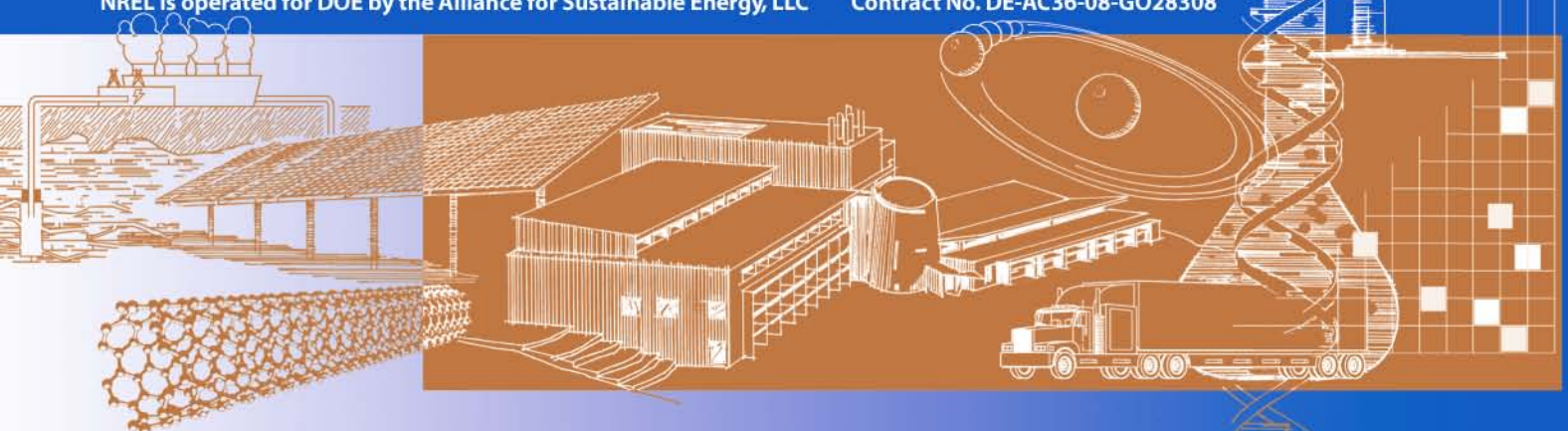

Available electronically at http://www.osti.gov/bridge

Available for a processing fee to U.S. Department of Energy and its contractors, in paper, from:

U.S. Department of Energy
Office of Scientific and Technical Information
P.O. Box 62
Oak Ridge, TN 37831-0062
phone: 865.576.8401
fax: 865.576.5728
email: mailto:reports@adonis.osti.gov

Available for sale to the public, in paper, from:

U.S. Department of Commerce
National Technical Information Service
5285 Port Royal Road
Springfield, VA 22161
phone: 800.553.6847
fax: 703.605.6900
email: orders@ntis.fedworld.gov
online ordering: http://www.ntis.gov/ordering.htm


Printed on paper containing at least 50% wastepaper, including 20% postconsumer waste

Durability of Poly(Methyl Methacrylate) Lenses Used in Concentrating Photovoltaic Modules

David C. Miller,* Lynn M. Gedvilas, Bobby To, Cheryl E. Kennedy, and Sarah R. Kurtz
National Renewable Energy Laboratory (NREL), 1617 Cole Blvd., Golden, CO, USA 80401

ABSTRACT

Concentrating photovoltaic (CPV) technology has recently gained interest based on their expected low levelized cost of electricity, high efficiency, and scalability. Many CPV systems use Fresnel lenses made of poly(methyl methacrylate) (PMMA) to obtain a high optical flux density. The optical and mechanical durability of such components, however, are not well established relative to the desired service life of 30 years. Specific reliability issues may include: reduced optical transmittance, discoloration, hazing, surface erosion, embrittlement, crack growth, physical aging, shape setting (warpage), and soiling. The initial results for contemporary lens- and material-specimens aged cumulatively to 6 months are presented. The study here uses an environmental chamber equipped with a xenon-arc lamp to age specimens at least 8x the nominal field rate. A broad range in the affected characteristics (including optical transmittance, yellowness index, mass loss, and contact angle) has been observed to date, depending on the formulation of PMMA used. The most affected specimens are further examined in terms of their visual appearance, surface roughness (examined via atomic force microscopy), and molecular structure (via Fourier transform infrared spectroscopy).

Keywords: Fresnel lens, PMMA, accelerated life testing, reliability, durability

1. INTRODUCTION

Concentrating photovoltaic (CPV) technology use relatively sizable optical component(s) to focus solar flux onto a relatively small photovoltaic (PV) cell. The CPV application becomes economically advantageous when the equipment cost is reduced by using optical components that are inexpensive relative to the PV cell. For example, the first component in a CPV system may be a Fresnel lens, composed of poly(methyl methacrylate) (PMMA). To realize low levelized cost of electricity, the optical components must provide good performance over the desired service life of 30 years. The advancement of high-efficiency PV cells, such as multijunction III-V technology [1], has recently motivated interest in CPV; however, understanding related to the durability of the optical components remains limited.

The durability of Fresnel lenses (with an emphasis on lenses made of PMMA) is being reviewed in [2]. Issues related to optical durability include increased optical absorptance, decreased bandwidth of the transmitted spectrum, and increased haze (caused by microcrazing and roughening of the first-surface). Mechanical durability depends on resistance to fracture, fatigue, physical aging (including creep and other dimensional instability), and solid erosion (particulate-mediated abrasion of the first-surface). The accumulation of particulate matter, known as natural soiling, is especially important in CPV, because it more adversely affects the direct solar flux transmitted through an optical system (whereas much of the scattered light is still useable in flat-panel PV applications). The weathering of PMMA may occur through the processes of photodegradation (mechanism of photolysis) and thermal degradation (mechanism of depolymerization via unzipping of molecular chains). Both may occur synergistically [2], aided by trace additives in the material formulation or residual monomer remaining from fabrication. Much of the literature examining the durability of PMMA is more than 20 years old [2], and few studies examine the material in the context of the CPV application. Further, many of the aspects related to mechanical, surface, and material considerations have been overlooked.

The goal of the study here is to examine the optical and mechanical durability of Fresnel lenses, using a variety of contemporary materials and lens (facet) designs. Specimens were subject to accelerated aging in a controlled environmental chamber. Contemporary specimens may be compared to veteran lenses, aged in the field. The study aims to examine traditional characteristics as well as additional seldom-examined characteristics, essential to the CPV application. This paper describes the initial results for 6 months of cumulative accelerated aging, with emphasis on optical durability. Mechanical characteristics will be examined in the future, at 1-year increments. The results for the indoor aging here will be compared to similar work in the literature, as well as to previous outdoor studies.

*David.Miller@nrel.gov; phone 1 303 384-7855; fax 1 303 384-6790; www.nrel.gov/pv/performance_reliability/

2. EXPERIMENTAL

Specimens examined include 11 varieties of stock (sheet) PMMA, one Fresnel lens with a linear focus, eight varieties of lenses with a spot focus, and three varieties of veteran spot-focus lenses. In most cases, the measurements were averaged for three replicate specimens. A wide variety of stock specimens, including formulations not necessarily intended for outdoor use, was purposely chosen here to more readily identify possible failure modes. The veteran lenses included those fielded in an urban desert environment (Phoenix, AZ) on a tracker for 8, 22, and 27 years. The veteran lenses were first measured in their as-received condition. These specimens were then cleaned with a 20% vol. solution of detergent (LiquiNox, Alconox Inc.) and deionized (DI) water prior to re-measurement. Except where noted, specimens were not subsequently cleaned prior to measurement.

Optical measurements were performed using a Lambda 900 dual-beam ultraviolet-visible-near infrared (UV-VIS-NIR) spectrophotometer (Perkin-Elmer Inc.) with a 60-mm-diameter integrating-sphere attachment. The hemispherical measurements, obtained using the integrating sphere, circumvent issues associated with Fresnel lenses, such as focal length and spot size. The entrance aperture of the integrating sphere is 30 mm and its incidence angle is 8°. The measurement accuracy of the instrument is ±0.08% in the UV/VIS and ±0.32% in the NIR, while the reproducibility is <2±0.8% (average±1 S.D.) [3]. To adequately monitor both UV and IR performance, transmission was measured from 200–2600 nm, for a 5-nm interval. The spectra obtained according to Ref. [4] can be later analyzed with the air-mass (AM) 1.5 terrestrial global solar spectrum [5]. In particular, the yellowness index (YI) was calculated for λ=380–780 nm from the transmittance measurements using the procedure [6] and ASTM D65-1964 coefficients to provide a single quantitative value that may be directly compared to visual appearance.

The specimens were photographed with a camera (40D, Canon Inc.), equipped with extension tubes, and white-balanced using a commercial filter (ExpoDisc 77 mm, ExpoImaging Inc.). A balance (A-200DS, Denver Instrument Co.), analytically accurate to ±0.1 mg, was used to weigh each specimen. A goniometer (100-00-115, Ramé-Hart Inc.), accurate to ±0.5°, was used for sessile drop measurements (*i.e.,* contact angle, for the left and right sides of the drop) using DI water. Measurements, taken once for each specimen, were then averaged for the replicate sets. Each specimen was cleaned with dry air prior to measurement to remove particulate contamination.

Specimens were aged in a Ci4000 Weather-Ometer (ATLAS Material Testing Technology LLC), operating at the chamber temperature of 60°C and relative humidity (RH) of 60%, rendering a black-panel temperature of 100 $\pm 7^0$C. (The local conditions for transparent polymeric specimens were previously verified at 70°C and 38% RH). Specimens were placed in a carousel that rotates about a continuously operating xenon-arc lamp. Borosilicate glass filters were used to filter the lamp so that it closely replicates the AM1.5 spectrum, with the power level being controlled to 114 $W \cdot m^{-2}$ for $300 \leq \lambda \leq 400$ nm, *i.e.*, 2.5x the AM1.5 global spectrum [5]. Instruments such as the Ci4000 provide an ~8x acceleration factor with respect to the UV dose (where additional acceleration related to the environmental conditions of temperature and RH is location specific), based on the optical flux and duration of exposure (24 hours/day). Specimens were aged for the cumulative durations of 0, 1, 2, 4, and 6 months, where one month corresponds to 30 days. Samples of a domed Fresnel lens (spot-focus), however, were aged at 85°C and 85% RH in the dark (Blue M FRS-361F, Thermal Product Solutions Corp.), because they could not be readily fitted to the standard Ci4000 specimen trays.

A Dimension 3100 (Veeco Instruments Inc.) atomic force microscope (AFM) was used to perform surface topography scans in tapping mode. The radius of curvature of the silicon NSC15/AIBS (MicroMasch Co.) tips used is nominally 10 nm with an included tip cone angle of 40°. The top surfaces of specific lens specimens were measured using 90x90 μm^2 then 20x20 μm^2 scans with 512 pixels in each direction (*i.e.,* ~180- or ~40-nm lateral resolution), which were then processed using the flatten and low-pass filter software features. Each specimen was examined along its length at the edge and center. Surface roughness (of the measured area) and the size of characteristic features (within a line scan) were determined using the instrument's software.

Fourier transform infrared (FTIR) spectroscopy was performed with a commercial spectrometer (Nicolet Nexus 870, Thermo Fisher Scientific Inc.). Attenuated total reflectance (ATR) spectra were obtained from 4000 to 650 cm^{-1} in 4-cm^{-1} increments, using a 50-mm x 10-mm x 5-mm ZnSe crystal attachment (ATR Max-II, PIKE Technologies). The sampling depth of the measurements is estimated to be on the order of 20 μm. For the measurements, an electronically temperature-controlled (ETC) mid-IR blackbody source (EverGlo, Thermo Fisher Scientific Inc.) was used as a light source while the crystal was held in place against the front (first) surface of each specimen.

3. DATA REDUCTION

All raw spectral measurements were subject to post-analysis. Accounting for all backward and forward reflections, the approximate transmittance through a thick flat-plate at each λ is given by Equation 1 [7].

$$T = \frac{\left(1-r_i\right)^2 e^{-h\alpha}}{1-\left(r_i^2 e^{-2h\alpha}\right)}, \text{ where } \alpha = \frac{4\pi k_2}{\lambda} \text{ and } r_i = \frac{\left(n_1-n_2\right)^2 + \hat{i}\left(k_1-k_2\right)^2}{\left(n_1+n_2\right)^2 + \hat{i}\left(k_1+k_2\right)^2} \quad (1)$$

Nomenclature, here for system international (SI) units, includes T, which represents the optical transmittance {unitless}; r_i, the reflectance at the interface {unitless}; h, the specimen thickness {m}; α, the absorption coefficient {m^{-1}}; π, the mathematical constant {3.142}; k, the extinction coefficient {unitless}; and n, the real component of the refractive index {unitless}. To clarify the nomenclature, the transmitted light is the remainder when the reflected (R) and absorbed (A) portions are subtracted from the incident flux (I), *i.e.*, $T=I-(R+A)$. The subscripts 1 and 2 distinguish between materials on opposite sides of the air interface. For a single material in air, $n_1 \rightarrow 1$ and $k_1 \rightarrow 0$. Following the method in Ref. [3], α was evaluated numerically every 5 nm, so that each transmittance measurement could be scaled to the common thickness of 3.175 mm, enabling direct comparison between specimens of different thickness ($1.4<h<5.3$ mm). To determine α, the n for PMMA was always taken from a curve fit, Ref. [3]. The wavelength at which the specimen became transmitting above –3dB (70.71%), $\lambda_{cut\ on}$ {nm}, was then calculated from the thickness-compensated data.

4. RESULTS AND DISCUSSION

4.1 Measurement of optical durability

Optical durability is examined in Figure 1 for the least-affected (#1), an intermediate (#8), and the most-affected (#11) of the stock specimen sets as ranked by YI. The spectra are shown for the initial (0 months) and most recent measurements (6 months). The normalized AM1.5 direct solar spectrum [5] is shown for reference. The specimen geometry is identified in the inset of the figure. A distinct reduction in the transmittance spectrum of set #11 is observed, where $\lambda_{cut\ on}$ evolves with time, from 320 to 615 nm. Transmittance is reduced for set#11 well above $\lambda_{cut\ on}$. A similar, but less pronounced effect is observed for set #1, where the originally distinct transition to transmission at 390 nm becomes attenuated, adopting a rounded profile. Here, a slight reduction in transmittance occurs in the transition region between ultraviolet (UV) and visible wavelengths. Separately, the transmittance is improved in the UV-B wavelengths (280–320 nm) for set #8. As in set #1, the transmittance of set #8 is reduced in the UV-A (320–400 nm) and visible wavelengths. Also, for set #8, a distinct peak originally observed at 310 nm becomes less discernable at 6 months. Quantitatively, the photon (γ) flux density in the application-specific wavelengths (λ=300–1800 nm) was decreased by 0.3% for set #8 after 6 months, whereas the optical flux density in the UV wavelengths (λ=280–400 nm) was increased by 18% over the same time period.

Regarding the infrared (IR) wavelengths, the standard absorption peaks for PMMA occurring at 1170, 1373, 1415, 1680, 1907, 1940, and 2130 nm (corresponding to 8547, 7286, 7067, 5952, 5242, 5155, and 4695 cm^{-1}, respectively) are observed for all of the profiles in Figure 1. These peaks correspond to overtones and combination bands of IR peaks occurring at lower wavenumbers (see Figure 9 below). No distinct effect of aging, however, is observed for any of the sets in the near-infrared (NIR) wavelengths. In comparison, the wavelength range commonly used in crystalline silicon cells is 300-1120 nm, whereas the range of 300-1800 nm is used in the more-efficient III-V multijunction PV cells.

The results in Figure 1 are primarily explained by the different formulations of material used. Set #11 is a specifically UV-transmitting (UV-T) PMMA formulation, allowing it to transmit the UV-B portion of the solar spectrum. Because it is UV transmitting, components made out of UV-T PMMA might be used in test fixtures examining material-specific UV-accelerated aging. This material does not contain UV absorbers, but it may contain other stabilization compounds. Components made of UV-T PMMA are shown here to have a limited lifetime in an accelerated-aging instrument (warranting periodic replacement), because they lose all UV transmittance with time. In contrast, set #1 demonstrates a stable profile. The vast majority of stock and lens specimens demonstrated profiles similar to set #1 at 0 and 6 months, including the $\lambda_{cut\ on}$ at 390 nm. For these specimens, the damaging dose of UV radiation occurring within a CPV system would be greatly attenuated relative to the nominal concentration of optical flux [3],[8]. The performance for set #8, where transmittance is both improved and degraded over separate wavelength regions, might be explained from the gradual depletion of additives (specifically, a component of the UV stabilization system). A time-dependent increase in

transmittance, particularly for the wavelengths just above the original peak at 310 nm, was observed for set #8 in the measurements at 1, 2, and 4 months (not shown). Ultimately, the optical transmittance of set #8 would be expected to degrade significantly if its stabilization system became exhausted. Reduced optical performance near the UV/visible transition is seen in the literature, in both indoor and outdoor facilitated experiments [2]. The profiles at 6 months for sets #8 and #11 might therefore be considered as more-pronounced demonstrations of the profiles ultimately expected for specimens subjected to prolonged aging.

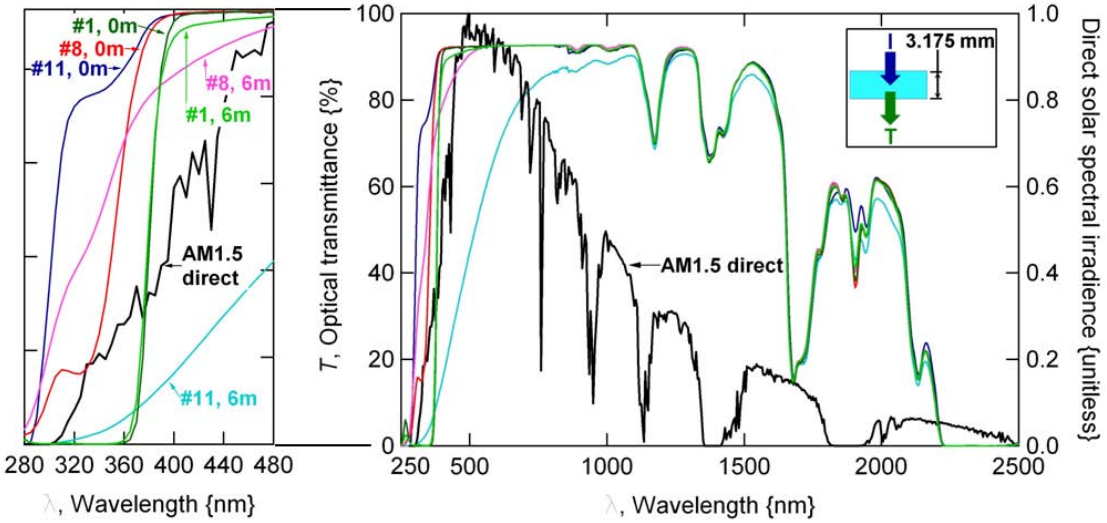

Figure 1: Measured optical transmittance (in air, compensated to h = 3.175 mm) for the least-affected (#1), intermediate (#8), and most-affected (#11) of the sets of stock specimens. The normalized direct solar spectral irradiance (AM1.5 in ASTM G173) is provided for reference.

All sets in Figure 1 demonstrate overlapping profiles in the IR region, particularly when compensated to h=3.175 mm. Peaks at 1.9 and 2.7 μm have been used in other polymeric materials to quantify water permeation with a spectrophotometer or IR detector [9],[10]. Although not shown, the difference spectrum for specimen set #1 (direct T of a specimen maintained in a dry box [≤0.1 ppm H_2O] minus that of an identical specimen soaked in DI for >1 month) demonstrated strong peaks at 1415, 1907, and 2697 nm (*i.e.*, 7067, 5244, and 3708 cm^{-1}, respectively) and lesser peaks at 2160 and 2955 nm (*i.e.*, 4630 and 3384 cm^{-1}, respectively); all of the aforementioned wavelengths are not used for energy production. The peaks below 2750 were separately verified in hemispherical measurements. Because PMMA may absorb up to 2.5% wt. water [2], the IR absorption peaks might be used to promptly analyze fielded components. Unfortunately, peaks exceeding the maximum λ of 2750 nm are beyond the measurement capability of conventional integrating spheres (used in hemispherical measurements), but may be examined in direct transmittance measurements of stock specimens up to the maximum λ of 3300 nm.

4.2 Influence of natural soiling on veteran fielded lenses

Results for the veteran lenses, measured in their as-received ("field") and "clean" conditions, are shown in Figure 2. The profiles for the most-soiled (fielded 22 years outdoors, "A"), and next-most-soiled (fielded 8 years, "B") sets are shown in the figure, with the third set of specimens (fielded 27 years, "C", not shown) being similar to set-B. Set-C was cleaned intermittently with a high-pressure water spray during its first 10 years in the field; the other specimens were never cleaned. A significant reduction in transmittance at all wavelengths is observed for set-A. Cleaning was found to significantly improve transmittance, particularly at shorter wavelengths for sets-B and -C. Quantitatively, the photon flux density in the application-specific wavelengths (see Table 1 below) was decreased by 15%, 2%, and 1% for the fielded veteran specimen sets (A, B, and C, respectively) relative to the cleaned condition. A rounding of the cut-on transition at $\lambda_{cut\ on}$=390 nm was observed for all of the veteran sets, similar to that occurring for set #1 in Figure 1. Quantitatively, the UV optical flux density was decreased by 29%, 6%, and 2% for the fielded veteran specimen sets (A, B, and C, respectively) relative to the cleaned condition. Initial T measurements of the veteran films were not possible; however, the similar profiles in Figure 2 relative to set #1 in Figure 1 suggest the veteran lenses have lasting optical durability.

Strong attenuation of the blue region is not apparent for either of the cleaned sets in Figure 2. Use on a tracker tends to reduce exposure to airborne contamination, particularly if the module is maintained ≥2 meters above the ground [11].

Sets-A and -B, mounted between 1 and 2 m above the ground, represent a less optimal installation. Enhanced absorptance is predicted according to a Mie scattering model [12], as the wavelength becomes comparable to particle size (the diameter commonly ranges from 1 to 40 μm for the particulate matter in the field [2]). The effect of wavelength-dependent attenuation in the CPV application would be to decrease the current generated in the topmost ("blue") cell in multijunction technology. That is, a red-shifted spectrum would render a current-limited condition at the top cell, reducing power yield. If soiling of the lens causes the current-limited condition, multijunction cells may undergo a greater loss in power yield than would be immediately suggested by the decreased photon flux density (for λ=300–1800 nm), because the cells are series connected. The reduction in transmittance in Figure 1 and Figure 2 under-represents current loss in CPV because it includes scattered (in addition to direct) optical flux.

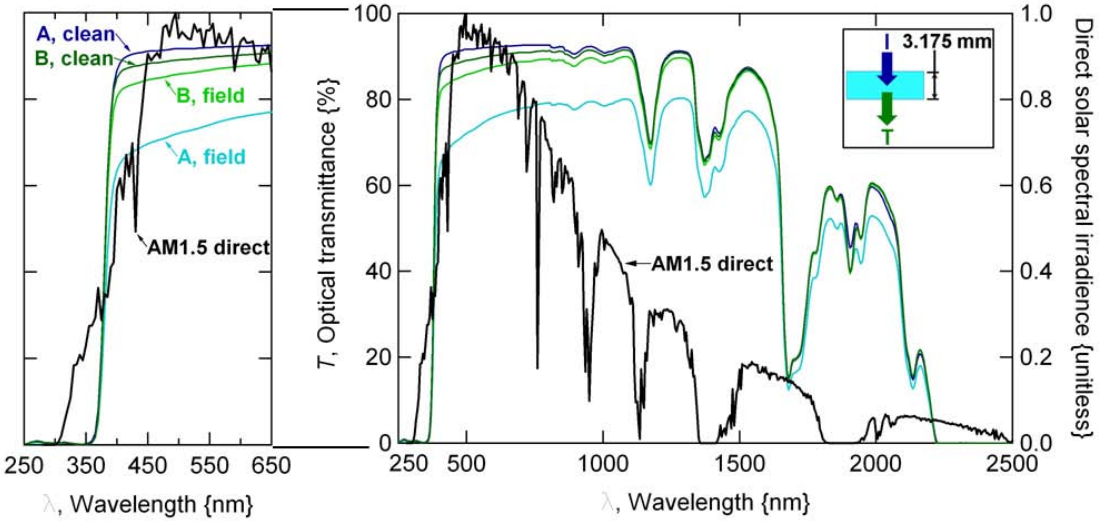

Figure 2: Measured optical transmittance (in air, compensated to h = 3.175 mm) for the most-soiled (fielded 22 years outdoors, "A") and next-most-soiled (fielded 8 years, "B") veteran lenses, relative to the normalized standard direct solar spectral irradiance [5]. Measurements were first made in the as-received condition and then after cleaning.

4.3 Additional results: yellowness index, mass loss, and data summary

The YI values, obtained from the transmittance measurements, are summarized in Figure 3. The data (with bounds for average ±1 S.D.) for the least-affected (set #1 in Figure 1), most-affected (#11 in Figure 1), and group average are shown for the stock specimens, in addition to that of the most-veteran (set-C, fielded 27 years) specimens. The same most-affected material (#11 in Figure 1, containing no UV absorber) was also subject to outdoor aging (on a tracker at Golden, CO), where the YI vs. cumulative field exposure time profile is shown in Figure 3. The initial (t=0) group average of YI=-1.2 is shown for reference, relative to the separate data profiles. The most-affected set (#11) is readily distinguished from the other indoor-aged specimens, which all lie between the least-affected and veteran profiles. From a least-squares fit, the slope of the most-affected set (#11, m=4.85) is 7.3x that of the average (m=0.66) and 35x that of the least-affected (#1, m=0.14). For sample #11, the difference between outdoor exposure and Ci4000 exposure is 220x that of the most-affected material, when aged outdoors (#11 outdoor, m=0.022). The cumulative exposure time for the outdoor aged specimen includes both sunny and cloudy days, with no active control of the ambient temperature or RH.

Figure 3 quickly distinguishes the most-affected specimen set from the others. From Figure 1, increased yellowness corresponds to reduced transmittance (and reduced optical bandwidth) at the shorter (blue) wavelengths. YI may therefore correspond to the formation of optically absorbing product species, including the chromophores contributing to continued degradation. Past studies suggest that much of the optical degradation occurs at the first-surface [2]. That is, transmittance was restored, approaching the original profile, when the first-surface was polished [13]. The substantially different damage rate (220x) between the indoor and outdoor aged specimen of the same material (#11), as well as the continued degradation of the veteran specimens may suggest a synergy between UV, temperature, and/or humidity. The results in Figure 3 more directly correspond with the visual appearance of the various specimens of different thickness, whereas thickness-compensated values (where h=3.175 mm, as shown in Figure 1 and Figure 2) may render an over-estimation of the absorbtance (particularly for the stock specimens, where h=1.39–4.05 mm).

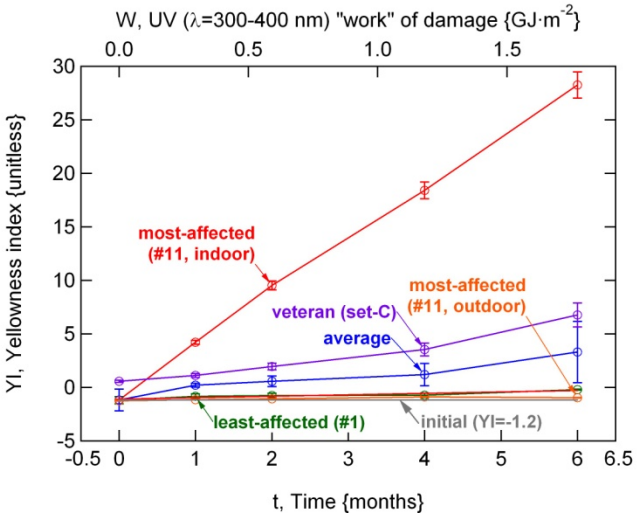

Figure 3: YI calculated directly from transmittance measurements for representative specimen sets. The least-affected (#1), most-affected (#11), and group average profiles are shown for the stock specimens, in addition to that of the most-veteran (set-C, fielded 27 years).

The loss of mass occurring during the first 6 months of the experiment is summarized in Figure 4. Unlike other characteristics, mass was not monitored until the completion of the first month, which is taken as the reference condition. The profile for the most-affected set in Figure 4 (corresponding to #11 in Figure 1) parabolically approaches 1.273%. The mass loss for set #11 exceeds others in the study, most of which are similar to the profile for the average of the stock specimen sets. The veteran lenses, represented by the most-veteran (set-C, fielded 27 years) specimens, demonstrate a profile overlapping the stock specimens. The mass of the most-affected material (#11 in Figure 1), when aged outdoors, varied considerably, suggesting the accumulation and loss of particulate matter.

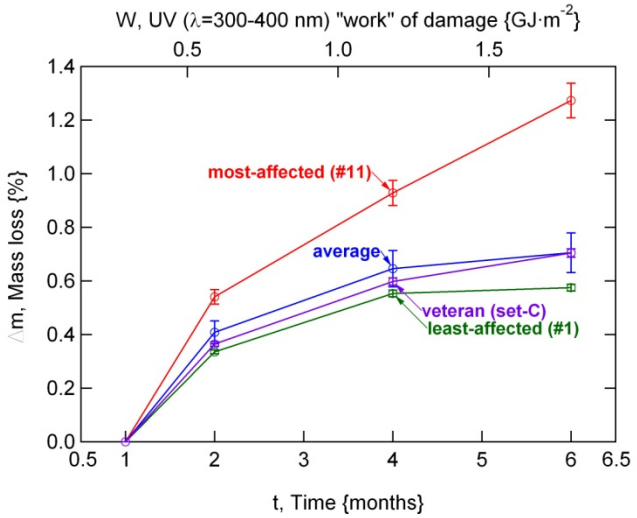

Figure 4: Mass loss for representative sets, relative to their "original" mass at 1 month. Data for the least-affected (#1), most-affected (#11), and average are shown for the stock specimens. Data for the most-veteran (set-C, fielded 27 years) are also provided.

The non-linear profiles in Figure 4 are readily distinguished from the linear profiles in Figure 3. Figure 4 suggests processes such as the outward diffusion of gaseous species or the depletion of residual components, *e.g.,* additives. Mass loss up to 4.35% was observed in a previous study [14], where other characteristics (observed using gel permeation chromatography and thermal mechanical analysis) indicated chain scission. The similar mass loss observed for both unaged and veteran specimens suggests material degradation, *i.e.,* a similar rate of depletion of residual components between specimens of such different history is unlikely. The mass loss in Figure 4 is expected to quantify the amount of

physio-chemical damage in each specimen, whereas the transmittance is affected non-linearly with depth in accordance with Beer's law (Equation 1) as well as the majority of the damage, presumed to occur at the first-surface [2].

Table 1 summarizes key characteristics for the stock specimen sets, including the photon flux density ($\varphi = \frac{q\lambda}{hc}\phi$ as in [3],[8]), the optical flux density ($\phi = \sum_{\lambda_i}^{\lambda_f} E[\lambda]T[\lambda]\Delta\lambda$ as in [3],[8]), YI, $\lambda_{cut\ on}$, mass loss (Δm), and contact angle (Θ). Additional parameters include: q, which represents the charge of a single electron $\{1.602\cdot10^{-19}$ C$\}$; h, Planck's constant $\{6.626\cdot10^{-34}$ W·s$^2\}$; c, the speed of light in a vacuum $\{2.998\cdot10^{8}$ m·s$^{-1}\}$; and E, the solar spectral irradiance $\{$W·m^{-2}·nm$^{-1}\}$. φ is analyzed using the AM1.5 direct solar spectrum [5], from λ=300–1800. Likewise, ϕ is analyzed from λ=280–400 nm and λ=1800–2600 nm, for the UV and IR wavelength regimes, respectively. Table 1 provides the values for the nine standard transmitting specimens (those that do not have enhanced or reduced UV transmittance characteristics). No strong trend with time is observed for φ, ϕ, or $\lambda_{cut\ on}$. As indicated in Figure 3, both the average and variation of YI increase with time. As indicated in Figure 4, the mass of the specimen sets decreases with time. Θ, which was first measured after 1 month exposure, also decreases with time. The data at 6 months were the exception. Here, the stock specimens were all cleaned (20% vol. LiquiNox in DI) prior to optical measurements because many had a hazy appearance. Without cleaning, it is expected that Θ would have been decreased at 6 months. In comparison, Θ for the combined sets of veteran specimens was 53±4° at 1 month, whereas Θ for the unaged stock specimens was 66±1°.

Table 1: Summary of key characteristics for the stock PMMA specimens. Values indicate the average ± 1 S.D. for the nine standard transmitting specimens. φ_{PV}, ϕ_{UV}, and ϕ_{IR} were calculated using the standard AM1.5 direct solar spectrum [5], from λ=300–1800 nm, 280–400 nm, and 1800–2600 nm, respectively.

		t, TIME {months}				
CHARACTERISTIC	UNIT	0	1	2	4	6
φ_{PV}	$\gamma\cdot m^{-2}\cdot s^{-1}$	723±3	724±3	721±4	725±3	719±6
ϕ_{UV}	$W\cdot m^{-2}$	14±8	17±8	17±7	17±8	16±9
ϕ_{IR}	$W\cdot m^{-2}$	7±0	7±0	7±0	7±0	7±0
YI	unitless	-1.2±0.1	0.2±1.4	0.6±1.4	1.2±1.7	3.3±2.9
$\lambda_{cut\text{-}on}$	nm	363±36	369±28	370±28	364±33	379±24
Δm, MASS LOSS	%	N/A	0.000±0.000	0.408±0.048	0.646±0.059	0.705±0.074
Θ, CONTACT ANGLE	degrees	N/A	66±1	60±1	58±2	61±4

Regarding Table 1, φ, ϕ, and $\lambda_{cut\ on}$ are expected to eventually show time-dependent trends. In particular, Figure 1 suggests that $\lambda_{cut\ on}$ will increase with time, causing the transmitted ϕ_{UV} to become attenuated. Because the UV spectrum may be harnessed by the PV cell, φ is also expected to become attenuated with time. However, the UV spectrum is a relatively small portion of φ_{PV}; therefore, the effect would be minor. No major change in the IR flux density is expected. Because the Ge ("red") cell is typically not current limiting, the effect of any change in ϕ_{IR} would be much less pronounced in a III-V cell than in a crystalline-Si cell. YI, which increases with time, supports the anticipated trends for φ, ϕ, and $\lambda_{cut\ on}$. The increased variability with time for YI suggests that the specimen sets studied here will ultimately be distinguished by a broad range of results. That is, the formulations of material are expected to degrade at separate rates.

Like YI, Θ importantly varies with time. Θ may be related to surface energy via the Young-Dupre equation [15], which characterizes the propensity for droplets– as well as monolayers–of water to adhere to the surface. The wetting of water relates to its ability to act as a cleaning agent, whereas the presence of monolayers relates to the process of capillary condensation, *i.e.*, a primary mechanism facilitating the adhesion of particulate matter [2]. A surfactant may be used to increase the effectiveness of cleaning by imparting a temporary, significant decrease in Θ. A prolonged decrease in contact angle, however, aids the accumulation of particulate matter. The decrease in Θ here is expected to relate to the chemistry and roughness of the surface. Aging within the Ci4000 has its limitations because the pH may differ significantly from that in the field and the additional characteristics of accumulated matter are not realized (although such matter tends to further lower the surface energy [2]). The Θ of the veteran lenses does suggest that the stock specimens will reach a future minimum value near 50°. The measurement at 6 months indicates that cleaning may impart

a temporary restoration of Θ, in some cases approaching the original value near 70°. This suggests the accumulation of a water-soluble species at the surface, which may result from the degradation of PMMA and/or its additives.

4.4 Examination of the most-affected specimens

Visual examination identifies characteristics that may ultimately render certain specimens unsuitable for the CPV application. Figure 5 compares the appearance of the least-affected (set #1 in Figure 1), most-affected (set #11), and increased-bandwidth (set #8) specimens. A yellow/brown discoloration is clearly evident for set #11; a lesser discoloration is barely discernable for set #8. At 6 months, the sets have the YI of 0.4, 28.3, and 5.2, respectively.

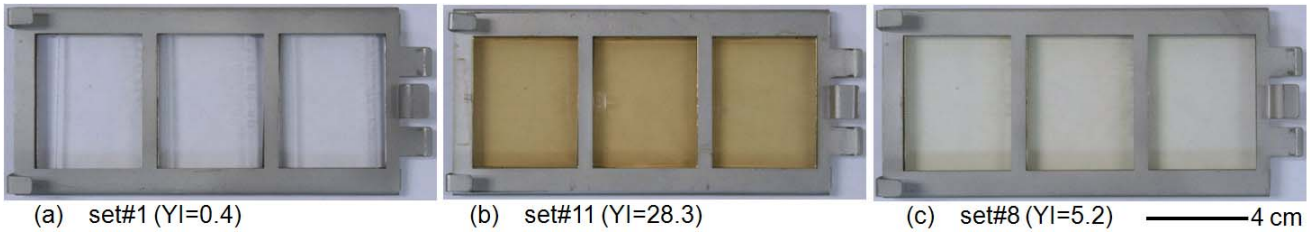

Figure 5: Visual appearance of specimen sets: (a) #1, (b) #11, and (c) #8 in Figure 1, from optical photographs (photographed in their mounting trays over white paper, and then subjected to a whiteness correction). The specimens have been aged for 6 months.

The domed Fresnel lens is examined in Figure 6. The main image, whiteness corrected as in Figure 5, identifies that no major discoloration has taken place (YI=-1.5). The photograph with a black background in the inset of Figure 6 more readily reveals the presence of cracks that extend perpendicular to the center of the specimen. The arrows in the figure identify a few of the cracks, which were present on all three replicate specimens. The feature in the center of the inset and the arc above and to its right are an artifact of manufacture present on all specimens. Not all of the cracks in Figure 6 originate from the center of the lens.

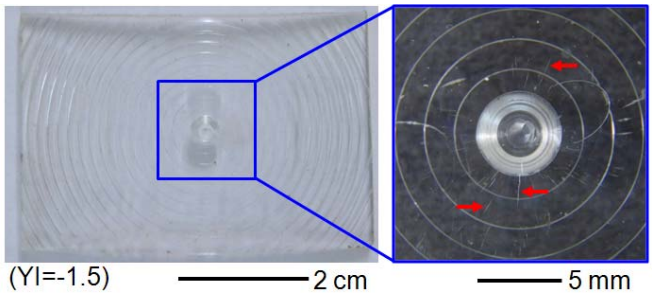

Figure 6: Optical images of a contemporary domed Fresnel lens specimen (aged for 6 months), where some of the radially oriented cracks present are identified with arrows in the inset.

The appearance of the veteran lenses is examined in Figure 7. Similar to the stock specimens at 6 months, a hazy white appearance was readily observed when looking through the specimens (not shown). To obtain images, a reflected light source was photographed at oblique angles. Specimen set-B (fielded 8 years) is represented in Figure 7(a) and set-C (fielded 27 years) in Figure 7(b). The affected surface appears in Figure 7(a) as mottled spots within the reflection of tubular-shaped lamp, whereas distinct features are visible across the surface in Figure 7(b). The images in Figure 7 were taken after the specimens were aged indoors for 6 months. The appearance of the as-received veteran specimens is not fundamentally different than that shown in the figure.

Regarding the appearances in Figure 5, Figure 6, and Figure 7, none automatically disqualify the respective specimens from use in CPV. The images do, however, suggest potential failure modes that could activate over time. The discoloration in Figure 5(b) lends perspective to the corresponding transmittance profiles in Figure 1. Although lesser discoloration in the other specimens is not problematic, the 16% loss in φ_{PV} for the specimen in Figure 5 (b) likely does disqualify it from use in CPV. Regarding the use of the same specimen in a multijunction CPV system, the 90% loss in ϕ_{UV} for this specimen suggests it would become current limited by the top (blue-absorbing) cell. Although the φ_{PV} for the specimen in Figure 5(c) is decreased by 0.3%, its reduced transmittance in the UV-B and blue wavelengths in Figure 1 suggests that the material may also limit the current in the top cell with continued aging.

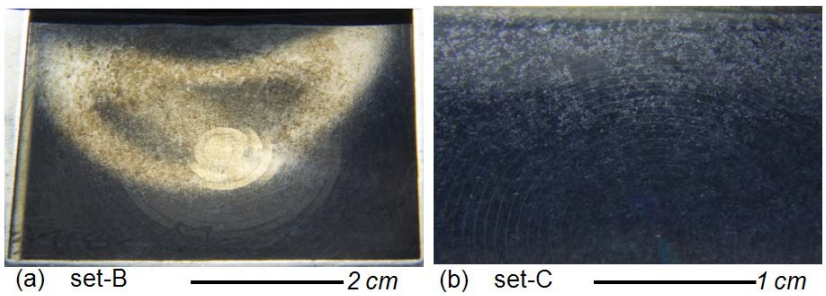

Figure 7: Optical images of veteran lenses (Figure 2) fielded: (a) 8 years, and (b) 27 years. Haze associated with the roughened front ("first") surface may be inferred from the heterogeneous regions of reflected light in (a) as well as the features observed at higher magnification in (b). Specimens are shown after 6 months of additional indoor aging.

No significant loss in transmittance was detected for the specimen in Figure 6; a few cracks, however, existed on the specimens at 6 months. The cracks likely originate from the residual stress remaining after manufacture, as well as the absorption of water and resulting mechanical hydro-expansion. Rapid cooling and high shear stress, common in the injection molding process, result in substantial residual stress [16]. Residual stress may be reduced through by using alternate manufacturing methods, such as hot-embossing. Defects at the surface may facilitate micro-crack formation, where the cracks may further grow when subject to cyclic stress. Fatigue may be driven by moisture absorption/desorption associated with weather events or by the heating/cooling associated with the diurnal temperature pattern, as well as discrete shading events. Unlike desert sites, coastal locations are prone to both moisture- and temperature-cycling. The cracks shown in Figure 6 are not likely to significantly compromise the CPV application. The cracks, however, may continue to grow until they mechanically compromise the lens during wind/snow-load or an impact event, *e.g.*, hail or rocks.

Figure 7 combines the considerations identified in Figure 5 and Figure 6. Optical hazing of PMMA lenses is often linked to a population of crazes and microcracks on the first-surface [2]. Optical hazing may also be facilitated by abrasion and solid erosion. Haze reduces optical transmittance and scatters light, producing greater optical loss than identified for the hemispherical measurements here. Furthermore, the microcracks may grow into macroscopic cracks (similar to Figure 6), potentially compromising the mechanical integrity of the lens. The majority of the haze in the veteran specimens is caused by solid erosion of the first-surface (Figure 8). The stock specimens, some of which show mild haze (not shown), are not subject to external abrasion in the Ci4000.

The first-surface of select specimens is represented in Figure 8. Specimens include #1 (from Figure 1, unaged), sets-B and -C (from Figure 2, cleaned after aging 8 or 27 years in the field), and set D (cleaned after aging 8 years in the field). The average ± root mean square (rms) ($R_a \pm R_{rms}$) and the peak-to-valley (R_{pv}) roughness are provided above each specimen. The scale of the topography varies with each image because it is tailored to discern the surface features. The surface in Figure 8(a), is relatively smooth (R=3±4 and 66 nm in 20x20 μm^2 scans), but exhibits some individual features, including surface waviness and discrete pits, *e.g.,* the 29- nm-deep pit in the image center. The surface in Figure 8(b) is the roughest (R=118±149 and 1,108 nm in 20x20 μm^2 scans). The specimens in Figure 8(c) and (d) demonstrate an intermediate roughness. Linear features are indicated with arrows in Figure 8(b) and (c), where they are not as readily apparent as in Figure 8 (d). The width (and depth) of the largest linear features is 3880 (340), 1540 (88), and 2350 (72) nm in Figure 8(b), (c) and (d), respectively. The overall surface texture was found to be similar between multiple sites, although the morphology of individual defects (such as pits) varied considerably.

The unaged specimen in Figure 8(a) will be referenced in comparison to the veteran lens specimens. Although the unaged specimen is not without surface features, it is significantly smoother than the veteran specimens. The rough surface in Figure 8(b), suggests solid erosion occurring in the field. The surface features there may consist of residual material from the lens (redistributed after kinetic impact) or embedded particulate matter. Unique modes were observed on that specimen in FTIR characterization, suggesting a different chemistry (*i.e.,* accumulated particulate matter). The linear nature and disparate orientation of the features in Figure 8(b), (c) and (d), suggests that they are scratches, likely to have originated during shipping and handling (sets-A, -B, and –C) or cleaning (set-D). The features are not expected to greatly affect the fracture strength of the lens, because their profiles (not shown) are rounded, *i.e.*, not sharp at the atomic scale. Figure 8(b) indicates that the haze in Figure 7(b) comes from solid erosion and not micro-cracks or scratches at the surface. A population of surface scratches, however, is detrimental to the direct solar flux focused by the lens.

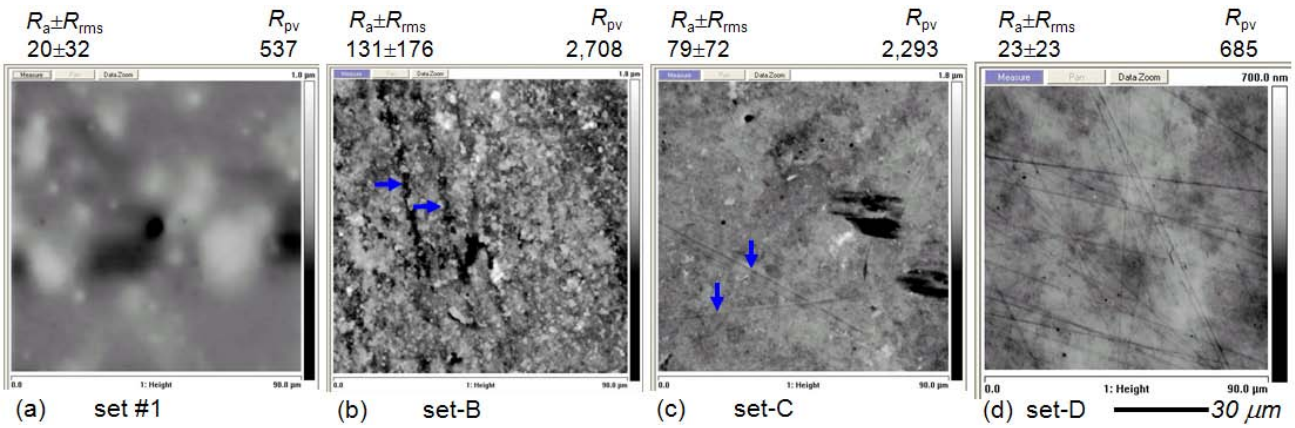

Figure 8: Surface topography scans of specimen sets: (a) #1 (unaged), (b) B (field-aged for 8 years), (c) C (field-aged for 27 years), and (d) D (field-aged for 8 years). The roughness of the scanned region ($R_a \pm R_{rms}$, averaged for two separate sites on each specimen, and R_p, the greatest measured) in nm is indicated above each image. Arrows indicate the location of surface scratches in (b) and (c).

4.5 Structural analysis using FTIR

The mechanism of degradation may be investigated using FTIR. For set #11, Figure 9 shows the spectrum of an unaged specimen relative to that of a specimen aged for 6 months. The profiles in the figure were obtained using the same scan settings for specimens of similar surface roughness. The spectrum for methyl methacrylate, from the Nexus 870 instrument library, is also shown for reference. Regarding the unit of measure (note different scale for the inset), the absorptance in Figure 9 is not the same as in the spectrophotometer measurements, *i.e.,* Figure 1 and Figure 2. Peaks are labeled in Figure 9 according to their location (wavenumber) and origin (corresponding molecular bond [17]). Many of the peaks correspond to modes of the carbonyl (C=O) or C-O bonds in the ester side group or the methylene ($-CH_2-$) structure on the backbone of PMMA. The major peaks in sets#1, -A, -B, and -C as in Figure 8 match those shown for PMMA in Figure 9. The locations of C=C peaks, indicative of unsaturated end-groups, are also labeled in Figure 9. C=C could remain from the polymerization process or form after photolysis or thermal degradation via disproportionation.

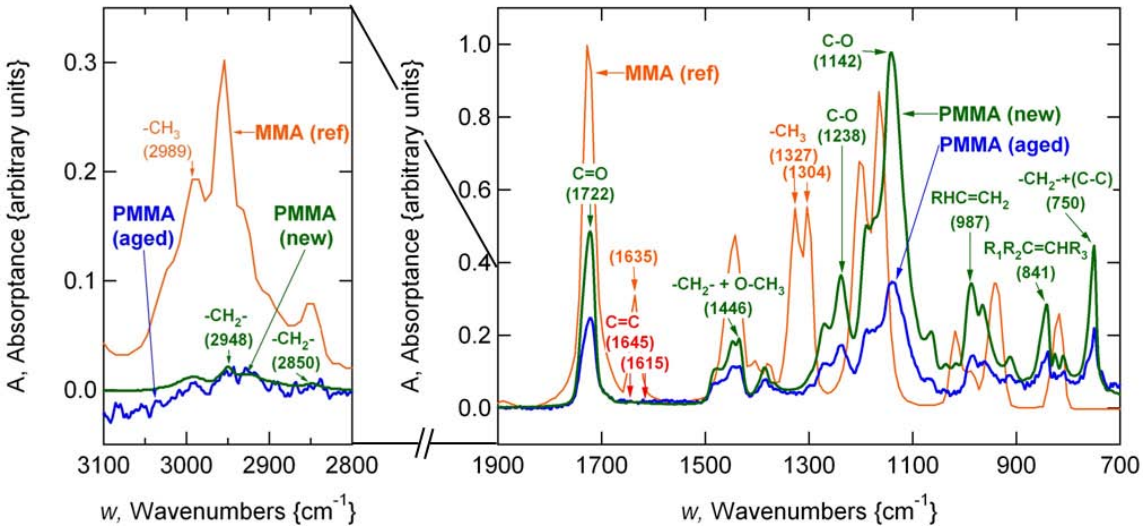

Figure 9: FTIR spectrum for specimen set #11 in Figure 1. The spectrum of a specimen aged for 6 months and that of an unaged specimen is shown relative to the reference spectrum for monomer (methyl methacrylate).

As a reminder, FTIR can identify damage to the molecular structure and/or the loss of additives occurring during aging. FTIR does not predict vulnerability to UV light or the IR wavelengths in Figure 9. The lack of characteristics specific to monomer (including unique peaks at w=1635, 1327, and 1304 cm^{-1} and enhancement of peaks at w=2948, 1722, and 1446 cm^{-1}) implies that it is not strongly present, as would be expected following depolymerization (chain unzipping) [2]. Instead, the relative magnitude of the peaks associated with methylene and the ester side-group are attenuated,

suggesting their population has been reduced. Unfortunately, this "signature" of chain scission is not a strong indicator because all of the prominent peaks for PMMA are associated with the ester and methylene groups. To explain, both are groups depleted simultaneously, rendering an intensity decrease throughout the spectra; no new peak occurs in the spectra as the result of chain scission. Although the spectrum in Figure 9 is consistent with chain scission, FTIR is not recommended for diagnosing the degradation of PMMA because of the lack of a strong indicator for chain scission. If the production of monomer is expected, however, FTIR may prove advantageous, provided timely measurement and/or cold (cryogenic) storage of specimens to limit the out-gassing of that volatile species.

5. CONCLUSIONS

The optical durability of poly(methyl methacrylate) Fresnel lenses has been examined with contemporary formulations and lens designs. By aging specimens in a Weather-Ometer, stock (sheet) as well as patterned lenses were examined relative to use in concentrating photovoltaic modules. The present work, which aims to identify adverse phenomenon that may occur during either qualification testing or the service life, does not include any catastrophic results. Key initial results, reported here after 6 months of cumulative exposure, include the following:

A range in the optical and mechanical durability of the various specimens was observed. For the most-affected specimen set, the wavelength at which the specimen became transmitting above -3dB increased from 320 to 615 nm, with an associated loss in the CPV specific photon flux density of 16% and loss in UV optical flux of 90%. In most other specimens, the cut-on wavelength remained at 390 nm, with only slight degradation of the UV transmittance. In a few specimens, the UV bandwidth was instead increased at minor expense (0.3% loss) to the CPV specific photon flux, attributed to depletion of the UV stabilization system. Particulate matter accumulated on veteran specimens decreased the CPV-specific photon flux and UV optical flux by as much as 15% and 29%, respectively. For soiled as well as optically degraded PMMA, the loss of transmittance at shorter wavelengths with time may eventually render a current-limited condition at the top cell, when multijunction technology is used.

The yellowness index of the most-affected specimen set increased linearly, at a rate 7.3x that of the average of the stock specimens. The 220x greater rate for the same material aged indoors (relative to the outdoor environment) suggests a synergy between UV, temperature, and/or humidity. The loss of mass, another indicator of degradation, increased asymptotically with time. The average mass loss of 0.7% is consistent with the loss of volatile species resulting from photolytic chain scission. Separately, the contact angle was found to decrease with time, from ~70° in unaged specimens to ~50° in veteran specimens. This implies the specimens will become more easily wetted during aqueous cleaning, but have become more prone to soil accumulation. The restoration of contact angle after cleaning at 6 months suggests the accumulation of water-soluble species at the surface. Such species may originate from the degradation of PMMA and/or its additives.

Visual inspection identified instances of overt discoloration, crack formation, and hazing. Residual and cyclic stress (hydro and thermal expansion) may facilitate macroscopic cracks, potentially compromising the mechanical integrity during wind/snow-load and impact events (hail or rocks). Optical haze, attributed to solid erosion of the front-surface of the veteran lenses, compromises direct transmittance. Surface characterization also identified scratches at the surface, attributed to cleaning. FTIR spectroscopy was consistent with the mechanism of chain scission. FTIR, however, is not a strong diagnostic tool here, because: (a) no strong scission-independent peaks exist for PMMA and (b) no strong peaks related to product species emerge after aging.

6. FUTURE WORK

The initial results of the durability study are reported here for review. Additional measurements will be performed in 6-month increments, up to the cumulative total of 36 months. At each of the cumulative 12-month periods, one of the specimens from each set will be retained for additional (destructive) characterizations including: haze (the difference between hemispherical and direct transmittance for the stock specimens), surface morphology (via atomic force- or scanning electron microscopy), facet geometry (electron microscopy, following cross-sectioning), indentation (which may identify hardness and toughness), rheometry (dynamic mechanical analysis), and calorimetry (verifying the glass-transition temperature). The characterization of mechanical properties and surface characteristics with aging, in particular, are notably absent from the CPV literature. Additional measurements may include X-ray photoelectron spectroscopy or Auger electron spectroscopy to examine the surface chemistry (proclivity to soil). Unfortunately, the shape of the specimen (which might have been characterized using optical interferometry to predict image aberration) is

not well suited to study here. This is because the spring force inherent to the specimen holders combined with the elevated temperature in the Ci4000 readily impart curvature, greatly exaggerating the effect of physical aging. Thus, it would be difficult to relate the behavior observed to date to that observed in the field, because the force applied by the specimen holders is not uniform within or between the specimen sets.

A second set of specimens is anticipated. For stock material, this would allow additional formulations to be examined so that a wider range of application-specific formulations may be compared. Additional lens specimens may be examined, including silicone-on-glass composite constructions. Lastly, additional outdoor-aged specimens would be included so that a location-specific acceleration factor may be obtained relative to the indoor aging.

ACKNOWLEDGEMENTS

The authors are grateful to Dr. Michael Kempe, Dr. Daryl Myers, Dr. John Pern, Matt Beach, Christa Loux, Marc Oddo, Bryan Price, Kent Terwilliger, and Robert Tirawat of the National Renewable Energy Laboratory for their discussion/help with the solar spectrum, experimental methods, optical measurements, or other subsequent analysis. This work was supported by the U.S. Department of Energy under Contract No. DE-AC36-08-GO28308 with the National Renewable Energy Laboratory.

REFERENCES

[1] R.R. King, A. Boca, W. Hong, X.-Q. Liu, D. Bhusari, D. Larrabee, K.M. Edmondson, D.C. Law, C.M. Fetzer, S. Mesropian, N.H Karam, "Band-Gap-Engineered Architectures for High-Efficiency Multijunction Concentrator Solar Cells", *Proc. PVSEC*, 55–61, (2009).

[2] D.C. Miller, S.R. Kurtz, "The Durability of Fresnel Lenses: A Review Specific to the Concentrating Photovoltaic Application", *in preparation*.

[3] D.C. Miller, M.D. Kempe, C.E. Kennedy, S.R. Kurtz, "Analysis of Transmitted Optical Spectrum Enabling Accelerated Testing of Multi-Junction CPV Designs", *in preparation*.

[4] "ASTM E903 Standard Test Method for Solar Absorptance, Reflectance, and Transmittance of Materials Using a Integrating Spheres," ASTM International, West Conshohocken, PA, 1-9 (1996).

[5] "ASTM G173 Standard Tables for Reference Solar Spectral Irradiances", ASTM International, West Conshohocken, PA, 1-20 (2003).

[6] "ASTM E313 Standard Practice for Calculating Yellowness and Whiteness Indices for Instrumentally Measured Color Coordinates", ASTM International, West Conshohocken, PA, 1-6 (2005).

[7] E.D. Palik, *Handbook of Optical Constants of Solids*, Academic Press Limited, London, (1998).

[8] D.C. Miller, M.D. Kempe, C.E. Kennedy, S.R. Kurtz, "Analysis of Transmitted Optical Spectrum Enabling Accelerated Testing of CPV Designs", *Proc. SPIE*, **7407**, 7407-16, 2009.

[9] J. Kapur, K. Proost, C.A. Smith, "Determination of Moisture Ingress Through Various Encapsulants in Glass/Glass Laminates, *Proc. IEEE PVSC*, 001210-001214 (2009).

[10] T. Swonke, R. Auer, "Impact of Moisture on PV Module Encapsulants", *Proc. SPIE*, **7412**, 74120A, (2009).

[11] J.P. Thornton, "The Effect of Sandstorms on PV Arrays and Components", *Proc. Solar*, 81-85, (1992).

[12] E.P. Roth, R.B. Pettit, "The Effect of Soiling on Solar Mirrors and Techniques Used to Maintain High Reflectivity", in *Solar Materials Science*, Academic Press: San Francisco, CA, 1980, 199-227.

[13] L.G. Rainhart, W. P Schimmel, "Effect of Outdoor Aging on Acrylic Sheet", SAND 74-0241, 1-41, (1974).

[14] M. Abouelezz, P.F. Waters, "Studies on the Photodegradation of Poly(methyl methacrylate)", NBSIR 78-1463, 1-55, (1978).

[15] W.D. Kingery, H.K. Bowen, D.R. Uhlman, *Introduction to Ceramics: Second Edition*, John Wiley and Sons: New York, NY, 1976.

[16] R. Leutz, L. Fu, H.P. Annen, "Stress in Large-Area Optics for Solar Concentrators", *Proc. SPIE*, **7412**, 741206 (2009).

[17] B. Smith, *Infrared Spectral Interpretation: A Systematic Approach*, CRC Press: Washington D.C., 1995.

REPORT DOCUMENTATION PAGE

Form Approved
OMB No. 0704-0188

PLEASE DO NOT RETURN YOUR FORM TO THE ABOVE ORGANIZATION.

1. REPORT DATE *(DD-MM-YYYY)*	2. REPORT TYPE	3. DATES COVERED *(From - To)*
August 2010	Conference Paper	

4. TITLE AND SUBTITLE
Durability of Poly(Methyl Methacrylate) Lenses Used in Concentrating Photovoltaic Modules: Preprint

5a. CONTRACT NUMBER
DE-AC36-08GO28308

5b. GRANT NUMBER

5c. PROGRAM ELEMENT NUMBER

6. AUTHOR(S)
D.C. Miller, L.M. Gedvilas, B. To, C.E. Kennedy, and S.R. Kurtz

5d. PROJECT NUMBER
NREL/CP-520-47604

5e. TASK NUMBER
PVD9.1320

5f. WORK UNIT NUMBER

7. PERFORMING ORGANIZATION NAME(S) AND ADDRESS(ES)
National Renewable Energy Laboratory
1617 Cole Blvd.
Golden, CO 80401-3393

8. PERFORMING ORGANIZATION REPORT NUMBER
NREL/CP-520-47604

9. SPONSORING/MONITORING AGENCY NAME(S) AND ADDRESS(ES)

10. SPONSOR/MONITOR'S ACRONYM(S)
NREL

11. SPONSORING/MONITORING AGENCY REPORT NUMBER

12. DISTRIBUTION AVAILABILITY STATEMENT
National Technical Information Service
U.S. Department of Commerce
5285 Port Royal Road
Springfield, VA 22161

13. SUPPLEMENTARY NOTES

14. ABSTRACT *(Maximum 200 Words)*

Concentrating photovoltaic (CPV) technology has recently gained interest based on their expected low levelized cost of electricity, high efficiency, and scalability. Many CPV systems use Fresnel lenses made of poly(methyl methacrylate)(PMMA) to obtain a high optical flux density. The optical and mechanical durability of such components, however, are not well established relative to the desired service life of 30 years. Specific reliability issues may include: reduced optical transmittance, discoloration, hazing, surface erosion, embrittlement, crack growth, physical aging, shape setting (warpage), and soiling. The initial results for contemporary lens- and material-specimens aged cumulatively to 6 months are presented. The study here uses an environmental chamber equipped with a xenon-arc lamp to age specimens at least 8x the nominal field rate. A broad range in the affected characteristics (including optical transmittance, yellowness index, mass loss, and contact angle) has been observed to date, depending on the formulation of PMMA used. The most affected specimens are further examined in terms of their visual appearance, surface roughness (examined via atomic force microscopy), and molecular structure (via Fourier transform infrared spectroscopy).

15. SUBJECT TERMS
Fresnel lens; PMMA; accelerated life testing; reliability; durability

16. SECURITY CLASSIFICATION OF:			17. LIMITATION OF ABSTRACT	18. NUMBER OF PAGES	19a. NAME OF RESPONSIBLE PERSON
a. REPORT	b. ABSTRACT	c. THIS PAGE			19b. TELEPHONE NUMBER (*Include area code*)
Unclassified	Unclassified	Unclassified	UL		

Standard Form 298 (Rev. 8/98)
Prescribed by ANSI Std. Z39.18